Acoustic Bragg Reflectors for Q-Enhancement of Unreleased MEMS Resonators

Wentao Wang, Dana Weinstein

HybridMEMS Lab, Massachusetts Institute of Technology
Cambridge, MA, USA
Email: wangwt@mit.edu

Abstract—**This work presents the design of acoustic Bragg reflectors (ABRs) for unreleased MEMS resonators through analysis and simulation. Two of the greatest challenges to the successful implementation of MEMS are those of packaging and integration with integrated circuits. Development of unreleased RF MEMS resonators at the transistor level of the CMOS stack will enable direct integration into front-end-of-line (FEOL) processing, making these devices an attractive choice for on-chip signal generation and signal processing. The use of ABRs in unreleased resonators reduces spurious modes while maintaining high quality factors. Analysis on unreleased resonators using ABRs covers design principles, effects of fabrication variation, and comparison to released devices. Additionally, ABR-based unreleased resonators are compared with unreleased resonators enhanced using phononic crystals, showing order of magnitude higher quality factor (Q) for the ABR-based devices.**

I. INTRODUCTION

The need for monolithic integration of Micro Electromechanical (MEM) devices with CMOS is critical for successful implementation of high frequency active MEMS resonators. Monolithic integration of these devices can provide basic RF and mm-wave building blocks with high Q, small footprint, and low power for use in wireless communication, microprocessor clocking, navigation and sensing applications. Nevertheless, the majority of MEMS resonators require a release step to freely suspend the moving structures. This necessitates complex encapsulation and packaging, restricting fabrication to MEMS-last or Back-End-of-Line (BEOL) processing of large-scale devices [1].

Toward the goal of Front-End-of-Line (FEOL) CMOS integration, the authors have previously demonstrated the first fully unreleased MEMS resonator operating at 39 GHz with Q of 129 [2]. The Si bulk acoustic resonator, surrounded on all sides by SiO_2, demonstrates the feasibility of direct integration of resonator into the FEOL CMOS processing, offering on-chip low power clock generation and high-Q tank filters.

Whether unreleased RF MEMS resonators are realized in a CMOS or custom process, their implementation provides high yield, low cost, robustness in harsh environments, and minimal or no-packaging solutions.
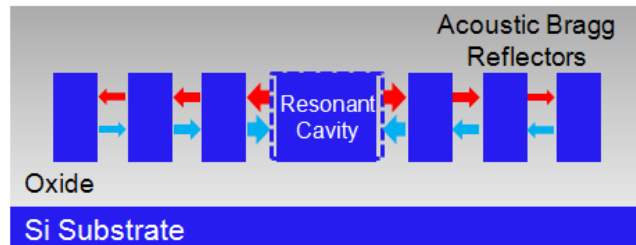

Figure 1. Sideview of unreleased resonator and ABRs lithographically defined in the same mask process. The resonant mode is longitudinal in the horizontal direction, exciting plane waves which are confined by the ABRs. Oxide cladding the resonator and ABRs illustrates the structures achievable in standard SOI CMOS processing.

As a result of the leakage of acoustic energy by wave paths into the surrounding medium, the performance of an unreleased resonator is degraded relative to its released counterpart [3]. This energy loss can be mitigated by adding acoustic isolation structures. In this work, two types of structures are proposed and investigated for the localization of acoustic vibrations in place of $\lambda/4$ suspension beams found in most released structures: the acoustic Bragg reflector (ABR) and the phononic crystal (PnC), with a focus on the former.

The acoustic Bragg reflector is named after its optical analogue, which is used as thin film optical mirrors to improve reflectivity at a designed wavelength. The ABR is composed of periodic layers of two materials of low and high acoustic impedance. At each layer interface of the ABR, a fraction of the acoustic wave energy is reflected. To form a coherent superposition of these reflected waves, these layers can be optimized at odd multiples of quarter wavelength, resulting in the overall reflectivity identical to that of free or rigid boundary conditions.

In 1965, W. E. Newell introduced the idea of employing ABRs to thickness mode piezoelectric resonators for wireless applications in high frequency integrated circuits [4]. This work was further developed in fully integrated surface micromachining technology for solidly mounted resonators (SMRs) [5]. These ABRs are composed of multiple depositions of alternating materials, resulting in acoustic isolation in one dimension at a single frequency per wafer. In-plane isolation can be achieved using lithographically defined

ABRs, as demonstrated in a suspended plate [6]. This configuration enables resonators of multiple frequencies to be fabricated side by side on the same chip.

PnCs provide an alternative solution to lithographically defined acoustic isolation. They have been recently explored by several groups for microscale applications, including acoustic mirrors for resonators in suspended plates [7], acoustic waveguides, and filters [8].

This paper presents the study of fully unreleased resonator surrounded by lithographically defined ABRs, embedded in a homogeneous cladding layer (Fig. 1). This one-mask design enables resonator banks of various frequencies on the same chip, providing multiple degrees of freedom in ABR design. With the goal of direct integration into FEOL CMOS processing, resonator performance is investigated for materials commonly found in the CMOS stack. The characteristics of these unreleased structures are compared with freely suspended resonators, released resonators isolated with lithographically defined ABRs, and PnC based unreleased resonators.

II. BANDGAP OF ACOUSTIC BRAGG REFLECTORS

Existing ABR analysis is based on a transmission line analogy, borrowing results from impedance transforming properties of cascaded transmission lines [4]. However, a more fundamental analysis can be performed conveniently from the wave propagation point of view through superposition, as shown in Fig. 2.

The acoustic impedance Z of an elastic medium for longitudinal wave is defined by material properties as

$$Z = \frac{E'}{c} = \sqrt{\frac{(1-\nu)\rho E}{(1+\nu)(1-2\nu)}} \tag{1}$$

where E, ρ, ν are the Young's modulus, density, and Poisson's ratio respectively.

In Fig. 2, an acoustic wave travelling to the right in material I is incident on an interface with material II, separated into reflected and transmitted components of R and T. At the next interface, the transmitted component T is reflected at an assumed lumped reflectivity of R' from the following stack of materials. The reflected wave now travelling to the left with amplitude TR' is then reflected (r) and transmitted (t) at the first interface. As a result, infinite reflections occur inside material II with amplitude decreasing in geometric progression. By summation of all the reflections, we acquire the recursion formula

$$R(n) = R + \frac{Ttr(n)e^{-i2\delta_2}}{1 - rr(n)e^{-i2\delta_2}} \tag{2}$$

in which δ_2 is the phase change over the propagation length in material II, $r(n)$ and $R(n)$ are the lumped reflectivities of the nth ABR bi-layer as shown in Fig. 2. Similarly, the other recursion formula can be acquired:

$$R = \frac{Z_1 - Z_2}{Z_1 + Z_2} \quad T = \frac{2Z_1}{Z_1 + Z_2} \quad r = \frac{Z_2 - Z_1}{Z_1 + Z_2} \quad t = \frac{2Z_2}{Z_1 + Z_2}$$

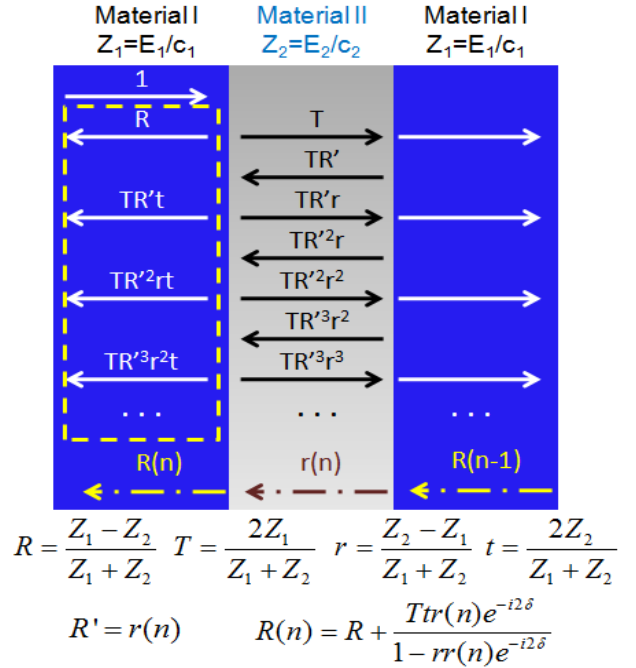$$R' = r(n) \qquad R(n) = R + \frac{Ttr(n)e^{-i2\delta}}{1 - rr(n)e^{-i2\delta}}$$

Figure 2. Derivation of recursion formula of reflectivity for ABRs through wave superposition. A summation of all the reflected components in the dashed line box generates relationship of lumped reflectivity R(n) and r(n) of the nth ABR bi-layer.

$$r(n) = r + \frac{tTR(n-1)e^{-i2\delta_1}}{1 - RR(n-1)e^{-i2\delta_1}} \tag{3}$$

With these two relations, the properties of the ABR can be extracted through numerical calculation. Fig. 3 shows the result of ABR reflectivity of various bi-layer numbers, in which the ABR bi-layer consists of Si and SiO$_2$.

An ideal ABR composed of an infinite number of bi-layers is approximated numerically using 100 ABR pairs. As shown in Fig. 3, this ideal ABR provides total reflection over several frequency ranges called the bandgaps. The reflectivity in the bandgap is strongly dependent on the number of ABR pairs. However, numerical results show that only 7 bi-layers are enough to approximate the bandgap shape, providing 98.7% reflectivity at the center of bandgap.

The convergence rate toward total reflection differs based on the materials composing the ABR structure. Material pairs with higher acoustic impedance contrast ratio (Z_1/Z_2) form a wider bandgap, and require fewer ABR pairs for same level of reflectance. The performance of several quarter-wavelength material pairs available in CMOS are exhibited in Fig. 4. The sign of reflectivity is determined by the order of materials in the ABR bi-layer. If the first material in the bi-layer has a higher acoustic impedance, the overall ABR will approach a free boundary condition (positive reflectivity). On the other hand, if the first material has a lower acoustic impedance, it will approach fixed boundary condition (negative reflectivity).

Materials of large acoustic impedance contrast such as W/SiO$_2$ [9], AlN/SiO$_2$ [5], Mo/Al [10] have previously been used to form ABR pairs in SMRs. This large contrast
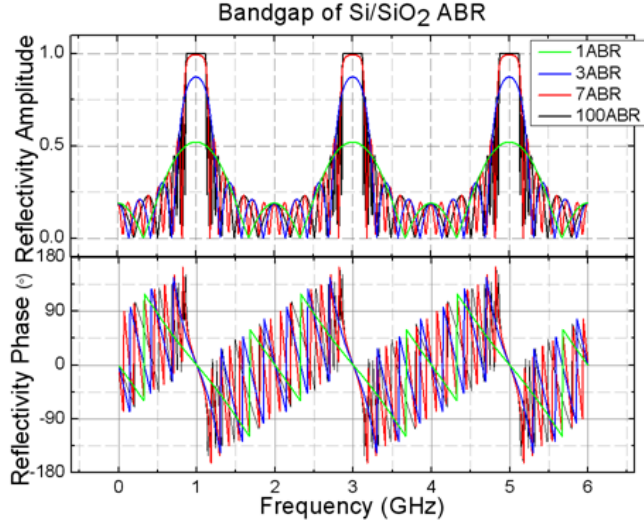
Figure 3. Frequency response of ABR amplitude (top) and phase (bottom). The bandgap approaches ideal shape with increasing number of ABRs. When the ABR pair number is small, the bandgap is attenuated and bandwidth increases.

minimizes the number of pairs required to achieve good acoustic isolation, reducing the number of deposition steps during fabrication. This will not complicate fabrication for unreleased resonator ABR design, since the entire ABR structure can be defined lithographically in one step. Si/SiO_2 ABRs are selected for the design and analysis in the paper, due to their FEOL CMOS compatibility, low internal loss, and small achievable footprint.

III. ACOUSTIC BRAGG REFLECTORS FOR UNRELEASED RESONATORS

The acoustic energy loss analyzed here in the unreleased resonators is analogous to anchor loss in freely suspended devices. In most released and unreleased resonators, this energy localization can be the limiting mechanism for Q. Accordingly, this analysis is focused on the mechanical

domain, taking maximum or average strain as signal output. This mechanical-only analysis in turn allows the result to be applied for various sensing mechanisms that rely on the electrical signal modulated by strain, such as dielectric, piezoelectric, piezoresistive, or Field Effect Transistor sensing [11].

A. 1D Analysis of Unreleased Resonator with ABRs

Using the superposition method outlined in section II, a one dimensional unreleased resonator embedded in an Si/SiO_2 ABR stack can be analyzed numerically using the maximum strain as the output (Fig. 5). This is a best-case ideal resonator output; in practical design the mode cannot be perfectly one-dimensional. Finite width may introduce non-idealities such as plate modes and extra wave leakage, as discussed in the following sections.

In this analysis, the resonator is excited by a pair of equal and opposite forces on both edges, and after superposing wave components in both directions, strain is calculated at the center of the resonator. Resonant peaks appear periodically at odd harmonics, which agrees well with the shape of the ABR bandgap. The Q of the peak increases rapidly with the increase of ABR pairs as the reflectivity approaches 1. These properties confirm the ABR analysis results in Fig. 3.

Because both the lengths of the ABR layers and resonant cavity are lithographically defined, the dimensions are subject to fabrication variations. Over-etching may change the relative thickness of the Si layer to the SiO2 layer in one ABR periodicity, which subsequently shifts performance of the entire system including frequency, Q, and amplitude of vibrations. However, the finite bandgap generated by the ABR provides some level of tolerance to such variations. Analysis indicates that fabrication tolerances of 10-15% results in up to 10% degradation in targeted performance. The fabrication variation affects performance more as the ABR pair number increases, which is reasonable due to the narrowing of equivalent bandgap as shown in Fig. 3.
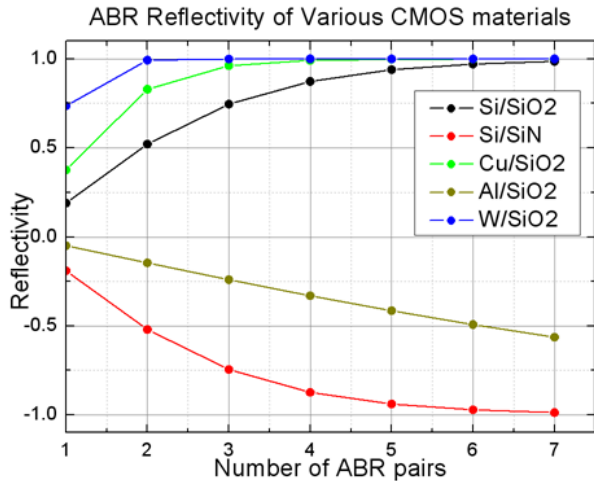

Figure 4. For finite number of ABR pairs, the reflectivity increases with the pair number and converges to 1 or -1 rapidly for materials commonly found in CMOS.
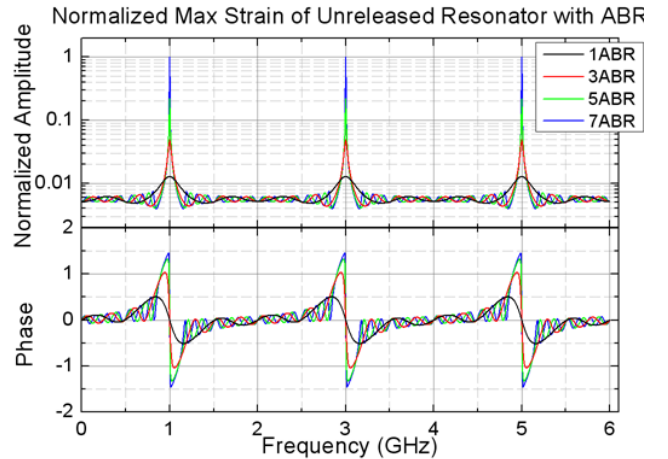

Figure 5. Numerical calculation results of maximum strain output of unreleased resonator embedded in ABR. The strain is normalized to the maximum strain at 7 ABR pairs.

B. Comparison of Released and Unreleased Resonator with ABRs

Two dimensional finite element simulations were performed in COMSOL Multiphysics 4.1 to demonstrate the contribution of ABRs to unreleased resonator performance. The frequency response of ABR-enhanced unreleased structures is compared with freely suspended resonators, simple unreleased resonators (no ABRs), and released resonators isolated with lithographically defined ABRs (Fig. 6). All resonators, driven by a pair of equal and opposite forces on both edges, are designed for 1st harmonic longitudinal vibrations at 1 GHz. The output signal is taken as the average strain across the entire resonant cavity. Perfectly matched layers (PMLs) are imposed at boundaries corresponding to energy sinks for waves propagating to infinity.

When defining PML parameters in COMSOL, it is recommended to match the PML to the desired acoustic wavelength. Although energy absorption is only optimized around the targeted wavelength, comparison of simulations with varying PML settings has shown robustness of PML performance over a broad range of frequencies for a single matched wavelength. For example, simulations of the resonator shown in Fig. 6(b, c) were performed with PMLs
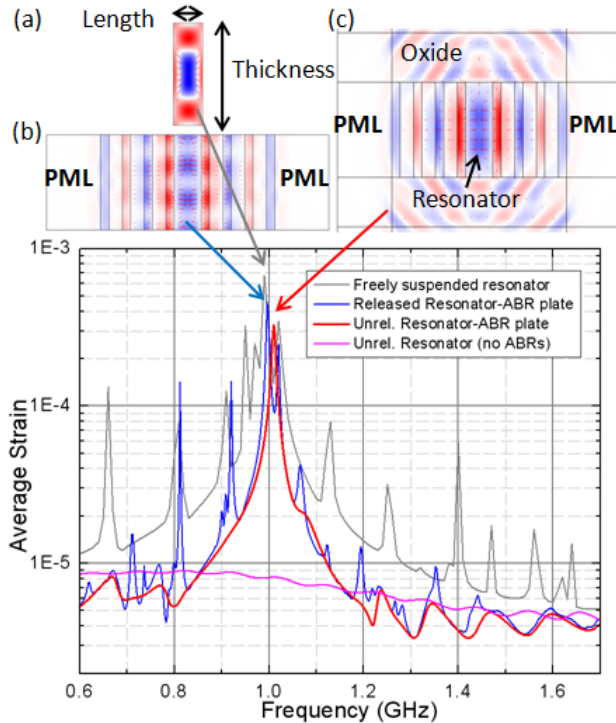

Figure 6. Frequency sweep in COMSOL for sideviews of free bar (a), released resonator-ABR plate (b), unreleased resonator-ABR structure embedded in oxide (c), and simple unreleased resonator embedded in oxide. Frequency response is for resonators of thickness-length ratio of 6.5 and ABR number of 7. Characteristic x-strain contour plots are given at an aspect ratio of 3.5 and ABR number of 3.

targeted at 1 GHz and 3 GHz wavelength, demonstrating maximum variation of less than 2% between the two simulations across a 3 GHz frequency sweep.

The released bar (Fig. 6(a)) provides the sharpest peak, which diverges for infinitesimal frequency steps due to the absence of internal damping in simulation. It is evident that due to the excitation of various plate modes, there are numerous spurious modes around the targeted frequency. At the other extreme, the unreleased resonator in oxide provides almost no peak at all, due to homogeneous energy dissipation into the surrounding medium. Comparison is made focusing on the released resonator-ABR plate (Fig. 6(b)) and the unreleased resonator-ABR structure (Fig. 6(c)). The output signal of the unreleased structure approaches that of the released one with increasing thickness-length aspect ratio. At an aspect ratio of 6.5, the unreleased resonator-ABR structure provides an output signal only 20% less than its released counterpart. The unreleased device also exhibits clear spurious mode suppression, providing a single peak at the desired frequency of 1 GHz.

Of all configurations, the unreleased resonator-ABR structure provides the purest mode due to damping of undesired plate modes in the non-resonant direction. Depending on the aspect ratio of the device, this out-of-plane damping may contribute to a reduced Q of the targeted mode, with a high aspect ratio being favorable for low loss. Nevertheless, it only requires an aspect ratio of approximately 7 for the output of unreleased resonator-ABR structure to match that of the released resonator-ABR plate. This effect results from the higher thickness uniformity of the mode present in the unreleased resonator (Fig. 6(c)), providing a larger effective area for sensing.

C. In-Plane ABR Design

To this point, analysis and optimization has been addressed for the sideview structure of both released and unreleased resonators. The lithographic definition of the ABRs under consideration affords a third degree of freedom in design to optimize for the quality factor and suppression of spurious modes. In the sideview case in the previous section, the resonator and ABRs are assumed to extend infinitely in the third dimension. In practice, the finite length of the structure introduces non-idealities and damping, which can be mitigated by in-plane ABR design.

Fig. 7 presents several in-plane ABR configurations for a 1D 2nd harmonic longitudinal-mode unreleased resonator. One half of the resonator is used for driving and the other half for sensing, providing maximum transduction area and selective excitation of the 2nd harmonic. As in the case of released resonator-ABR plate, the extra reflectors result in standing waves in the direction perpendicular to the longitudinal wave, causing signal cancellation and reduction in Q relative to the case of the infinite structure. Inclusion of corner ABRs also introduces spurious plate modes as exhibited in the inset in Fig. 7.
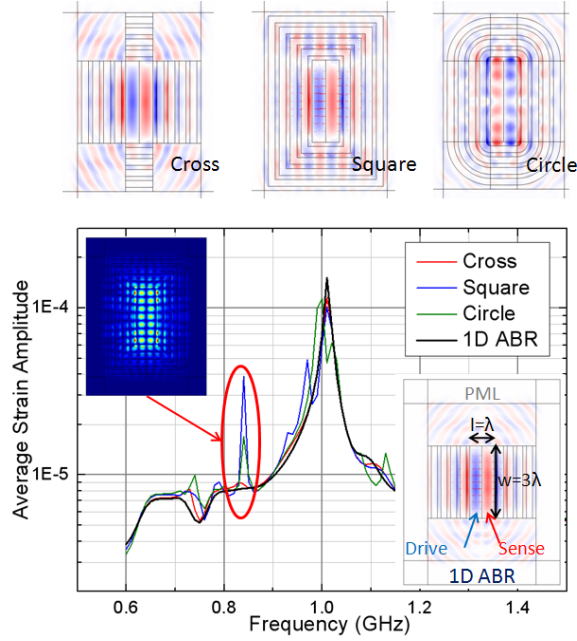
Figure 7. Frequency sweep around the 2nd harmonic in COMSOL on layout designs of cross, square, circular and 1D ABR structures (topview). Adding ABRs for longitudinal waves on the sides of the resonator does not enhance Q. Instead, it tends to introduce spurious modes. The inset presents the spurious mode for the square layout.

This result suggests that the 2D ABR design should serve to minimize any extra 2D in-plane vibrations and target a single mode. In the case of the longitudinal-mode resonator with 1D ABRs, in order to localize energy without mode distortion, side reflectors should coherently reflect only shear waves rather than longitudinal waves (Fig. 8). The shear reflectors do not act as standing wave boundary conditions to distort the 1D longitudinal mode, thereby providing higher Q and larger output signal.

This enhancement is more evident for higher harmonics. The reduced wavelength of the 6th harmonic in Fig. 8 results in
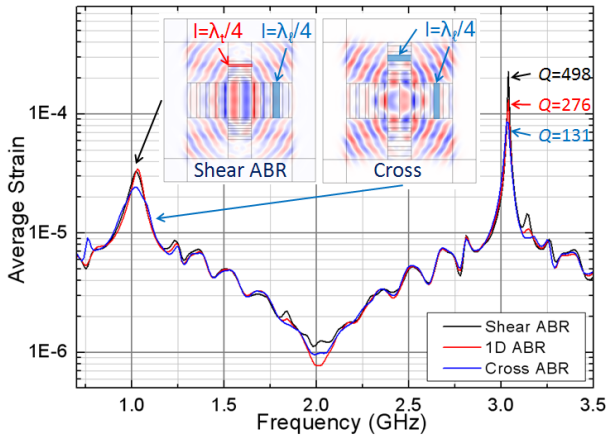

Figure 8. Frequency sweep in COMSOL including the 2nd and the 6th harmonic on unreleased resonator with side reflectors (topview). The width-length aspect ratio of the unreleased resonator is 1.5. Designing side reflectors at quarter shear wavelengths provides more uniform mode and larger signal output.

a more uniform mode along the width of the resonator. In this case, the vibrations near the sides of the resonator are increased such that the contribution from the side ABRs is larger. As can be seen in Fig. 8, the 6th harmonic at 3 GHz exhibits a significantly larger amplitude and higher Q than the 2nd harmonic at 1 GHz due to the increased width to wavelength ratio. In this case, the shear ABRs also serve to enhance the Q by a factor of 2 relative to the 1D ABRs and by a factor of 4 relative to the cross configuration. This quality factor can be further enhanced by increasing the thickness-to-height aspect ratio of the resonator and surrounding ABRs.

IV. ACOUSTIC BRAGG REFLECTORS VS. PHONONIC CRYSTALS

The ABR can be understood as one dimensional case of the phononic crystal (PnC). The PnC is an acoustic wave analogue of photonic crystals, where a periodic array of scattering elements in a homogeneous matrix material causes complete rejection of acoustic waves at a band of frequencies. Much attention has been drawn to the implementation of PnCs for MEMS resonators. One widely used structure is an in-plane wave transmission line resonator analogous to the Fabry–Pérot interferometer [7]. Typically, air holes are etched as scattering elements in a silicon slab (or slab made of other materials) to form a PnC structure. There are also solid scattering approaches to fill these holes with materials with distinct acoustic impedance from the slab [12].

Solid scattering design can be utilized to localize vibrations in unreleased resonators. To compare the performance of a 1D ABR structure to that of a PnC, a silicon square lattice PnC with oxide scattering elements is considered. The fabrication process would be identical to that of the ABR, except for a change in layout, with holes in place
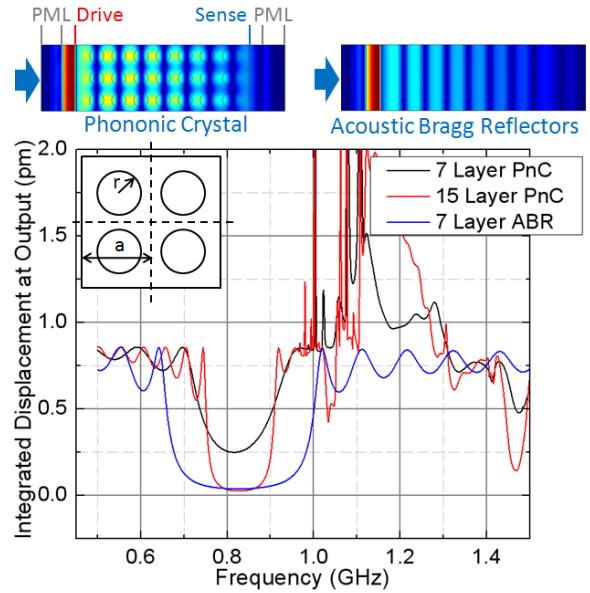

Figure 9. Acoustic bandgap comparison between phononic crystal and acoustic Bragg reflectors. The ABR provides a wider bandgap with no eigenmodes beyond the bandgap, and it requires a smaller footprint. The inset shows a 2x2 unit cell for the PnC used in this analysis. The contour plots show the topview of the transmission line structure, with amplitude of displacement decreasing with penetration depth.

of trenches defined by lithography. Similarly to the ABR, the central frequency of the bandgap for the PnC is dominantly dependent on periodicity, or lattice constant 'a', which approximately equals a half wavelength, while the width of bandgap is related to the filling ratio r/a (Fig. 9, inset). A COMSOL parameter sweep of the bandgap with respect to filling ratio shows the widest bandgap at filling ratio of ~0.3 for Si/SiO_2.

To compare the bandgap formed by the ABR and PnC, a transmission line configuration is investigated in COMSOL, with acoustic excitations generated on the left-hand side and sensing on the right, enclosed in PMLs on both ends (Fig. 9). Periodic boundary conditions are added on top and bottom so that the bandgap property is not distorted by the width dimension. The comparison result shows that the ABR has several advantages over the PnC for unreleased resonators:

- ABRs provide a much wider bandgap than that of PnCs for given impedance contrast of materials and for the same footprint.

- To achieve a near-perfect bandgap, it requires much fewer layers for the ABR compared to the PnC, requiring a smaller footprint.

- At frequencies beyond the bandgap, there exist spurious eigenmodes for the PnC, which results in undesired strong resonance. On the other hand, the ABR provides a perfect bandgap without introducing spurious modes.

As an outcome of these advantages, for the same footprint and material set, if we compare the PnC or ABR applied to an unreleased resonator driven on both ends, the ABR offers clear benefits, with a 9x higher Q, 20x larger signal output, and suppression of spurious modes at both low and high frequency (Fig. 10).
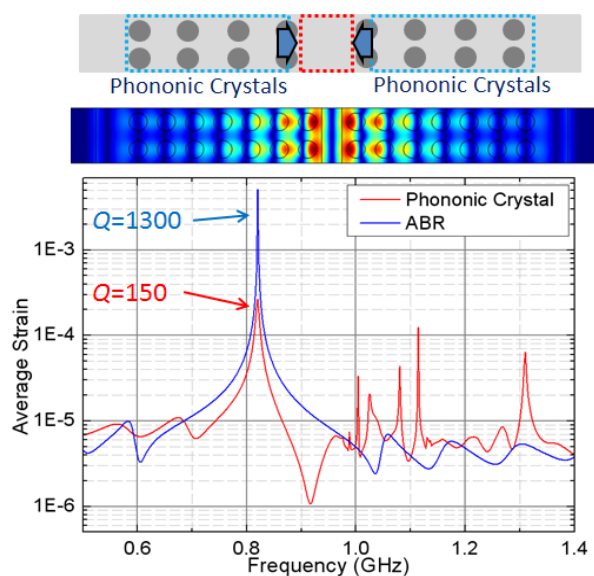

Figure 10. Comparison of performance of unreleased resonator embedded in the PnC and ABR. The contour plot is a topview simulation result in COMSOL with periodic boundary condition added on top and bottom. A pair of equal and opposite forces is applied on both edges of the resonator.

V. CONCLUSIONS

The design of the unreleased resonator with ABRs was optimized to suppress spurious modes and enhance the quality factor. With sufficient thickness-to-length aspect ratio, the unreleased design is able to provide signal level and Q that are comparable to its released counterparts. At high frequencies (>1 GHz) where resonator damping is dominated by anchor loss [13], the unreleased resonator with ABRs can outperform released devices.

Since the ABRs are lithographically defined in the same step as the resonator itself, their fabrication does not require any additional depositions or masks. In addition, it enables flexibility in ABR layout configuration, which can be implemented to optimize the ABR geometry for a single mode, resulting in high Q design with a finite footprint. Compared with the PnC, the ABR is more efficient in acoustic energy localization both in performance and footprint, and does not introduce any spurious modes.

The design of unreleased resonators enhanced with acoustic Bragg reflectors can provide basic building blocks for RF circuit designers with high-Q on-chip signal generation and processing that can be directly integrated into the FEOL in CMOS processing. Unreleased design also provides high yield, low cost, robustness in harsh environments, and minimal or no packaging for MEMS resonators.

REFERENCES

[1] G.K. Fedder, R.T. Howe, T.-J. King Liu, E.P. Quevy, "Technologies for cofabricating MEMS and electronics," *Proceedings of the IEEE*, **96**(2), 306-322 (2008).

[2] W. Wang, L.C. Popa, R. Marathe, D. Weinstein, "An unreleased mm-wave resonant body transistor", *IEEE MEMS*, 1341-1344 (2011).

[3] D. Weinstein, S.A. Bhave, "Acoustic resonance in an independent-gate FinFET," *Hilton Head MEMS Workshop 2010*, 459-462 (2010).

[4] W.E. Newell, "Face-mounted piezoelectric resonators," *Proceedings of IEEE*, **53**(6), 575-581 (1965).

[5] K.M. Lakin, "Thin film resonators and filters," *IEEE Ultrasonics Symposium 1999*, 895-906 (1999).

[6] R.H. Olsson , J.G. Fleming, M.R. Tuck, "Contour mode resonators with acoustic reflectors," US patent 7385334 B1 (2008).

[7] S. Mohammadi, A.A. Eftekhar, W.D. Hunt, A. Adibi, "High-Q micromechanical resonators in a two-dimensional phononic crystal slab," *Applied Physics Letters*, **94**, 051906 (2009).

[8] R.H. Olsson, I. El-Kady, "Microfabricated phononic crystal devices and applications," *Measurement Science and Technology*, **20**, 012002 (2009).

[9] S. Marksteiner, J. Kaitila, G. Fattinger, R. Aigner, "Optimization of acoustic mirrors for solidly mounted BAW resonators," *IEEE Ultrasonic Symposium 2005*, 329–332 (2005).

[10] J. Enlund, D. Martin, V. Yantchev, I. Katardjiev, "Solidly mounted thin film electro-acoustic resonator utilizing a conductive Bragg reflector," *Sensors and Actuators A*, **141**, 598-602 (2008).

[11] D. Weinstein, S.A. Bhave, "The resonant body transistor," *Nano Letters* **10**(4), 1234-1237 (2010).

[12] R.H. Olsson III, J.G. Fleming, I.F. El-Kady, M.R. Tuck, F.B. McCormick, "Micromachined bulk wave acoustic bandgap devices," *IEEE Transducers 2007*, 317-321 (2007).

[13] R. Tabrizian, M. Rais-Zadeh, F. Ayazi, "Effect of phonon interactions on limiting the f.Q product of micromechanical resonators," *IEEE Transducers 2009*, 2131-2134 (2009).